Reactions over Multiple, Interconnected Potential Wells: Unimolecular and Bimolecular Reactions on a C_3H_5 Potential†

James A. Miller* and Juan P. Senosiain

Combustion Research Facility, Sandia National Laboratories, Livermore, California 94551-0969

Stephen J. Klippenstein and Yuri Georgievskii

Chemical Sciences and Engineering Division, Argonne National Laboratory, 9700 South Cass Avenue, Argonne, Illinois 60439

Received: May 21, 2008; Revised Manuscript Received: July 2, 2008

In this article we analyze quantitatively and discuss in detail a number of reactions that take place on a C_3H_5 potential. These reactions include the reaction of hydrogen atoms with allene and propyne, the reaction of methyl with acetylene, the isomerization of cyclopropyl to allyl, and the dissociation of allyl, 1-propenyl, and 2-propenyl. The theory employs high-level electronic-structure methods to characterize the potential energy surface, RRKM theory to calculate microcanonical, *J*-resolved rate coefficients, and master-equation methods to determine phenomenological rate coefficients, $k(T,p)$. The agreement between our theory and the experimental results available is very good. The final theoretical results are cast in a form that is convenient for use in chemical kinetics modeling.

Introduction

The original intent of this investigation was simply to obtain a good rate coefficient for allyl (CH_2CHCH_2) dissociation over a wide range of temperatures and pressures. However, the C_3H_5 potential energy surface (PES) contains a wealth of kinetic information, notably for the reactions,

$$H + C_3H_4a \rightleftarrows H + C_3H_4p$$

$$H + C_3H_4p \rightleftarrows CH_3 + C_2H_2$$

$$H + C_3H_4p \rightleftarrows C_3H_3 + H_2$$

$$H + C_3H_4a \rightleftarrows C_3H_3 + H_2$$

and

$$c\text{-}C_3H_5 \rightleftarrows CH_2CHCH_2$$

as well as the dissociations of the allyl, 1-propenyl, and 2-propenyl radicals. In the reactions above C_3H_4a is allene, C_3H_4p is propyne, C_3H_3 is propargyl, and $c\text{-}C_3H_5$ is cyclopropyl. To varying extents all these reactions play a role in the chemistry of rich flames that leads to the formation of aromatic compounds, polycyclic aromatics (PAH), and soot.[1−7] They are particularly important in laboratory flame experiments in which allene or propyne is the fuel.[8] Consequently, we decided to extract all the information we could about these reactions. This task is relatively straightforward using the master-equation (ME) methodology we have developed over the past few years.[9−16]

The reactions of concern to us in this article have been studied both experimentally and theoretically a number of times in the past,[17−44] perhaps most notably in connection with photodissociation experiments.[34−44] Our work is closest in spirit to that of Davis et al.[17] and Wang et al.[33] Although our electronic-structure and dynamical methods (variational transition-state theory) are modest improvements over the methods employed in these previous investigations, the master-equation methodology used here is a vast improvement over the modified-strong-collider approach used in previous work. Our own experience is that, in general, modified-strong-collider predictions are in poor agreement with ME results when the same energy transfer model is used in both. The present investigation is also broader in scope than previous efforts.

Theoretical and Computational Approach

The B3LYP hybrid DFT (density functional theory) method was employed with Pople's split-valence 6-311++G(d,p) basis set to optimize geometries and compute the vibrational frequencies of all the relevant stationary points on the PES, both minima and saddlepoints. Additionally, we calculated rotational potentials for molecular configurations with internal rotations, intrinsic reaction coordinate (IRC) curves, and projected frequencies along these curves for the association/dissociation channels using this theoretical model. To obtain accurate rate coefficients, we also calculated single-point energies at all the stationary points and points along the IRC curves using Dunning's basis sets, cc-pVxZ with x = T, Q, and the rQCISD(T) method (spin-restricted quadratic-configuration-interaction with perturbative estimate of the triples contribution). Finally, the latter energies were extrapolated to the infinite-basis-set limit using the formula[45,46]

$$E(\infty) = E(l_{max}) - B/(l_{max} + 1)^4$$

where l_{max} is the maximum angular momentum in the basis set and B is a fitting constant.

Phenomenological (thermal) rate coefficients, $k(T,p)$, were determined as a function of temperature and pressure using 3 different forms of the master equation:[9]

1. The time-dependent multiple-well ME. This approach is limited to a one-dimensional formulation in which *E*, the vibrational−rotational energy of the molecule or complex, is the independent variable.

† Part of the "Stephen R. Leone Festschrift".

* Corresponding author. E-mail: jamille@sandia.gov.

10.1021/jp804510k CCC: $40.75
Published on Web 08/20/2008

TABLE 1: Results of Electronic Structure Calculations

	B3LYP/6-311++G(d,p)			QCISD(T) *E* (hartrees)			
	E(hartrees)	ZPE(hartrees)	⟨*S***2⟩	cc-pvtz	cc-pvqz	*E*/inf+ZPE (kcal/mol)	T1 diagnostic
$C_3H_4a + H$	−117.1976604	0.054857	0.0, 0.75	−116.93356	−116.96696	0 (reference)	0.0127, 0.000
$C_3H_4p + H$	−117.1951071	0.055482	0.0, 0.75	−116.935537	−116.969151	−1.0753707	0.0119, 0.000
$CH_3 + C_2H_2$	−117.2118501	0.054928	0.7534, 0.0	−116.948773	−116.981981	−9.2968114	0.0059, 0.0135
$c\text{-}C_3H_4 + H$	−117.1566074	0.055706	0.0, 0.75	−116.898028	−116.931637	22.608127	0.0103, 0.000
$C_3H_3 + H_2$	−117.2193285	0.051082	0.7700, 0.0	−116.9512237	−116.9849548	−13.80458122	0.0234, 0.0058
allyl	−117.2982738	0.065834	0.7779	−117.032952	−117.066556	−55.69807	0.0108
CH_3CCH_2	−117.2657109	0.065074	0.7589	−117.001004	−117.034505	−36.017353	0.0151
CH_3CHCH-trans	−117.2578223	0.065518	0.7595	−116.995124	−117.028476	−31.890684	0.0147
CH_3CHCH-cis	−117.2585198	0.065333	0.7594	−116.995683	−117.02906	−32.384604	0.0149
$c\text{-}C_3H_5$	−117.2486144	0.066337	0.7532	−116.986728	−117.020276	−26.316947	0.0124
ts1	−117.193083	0.056307	0.7654	−116.926699	−116.960557	4.7285714	0.0161
ts2	−117.1886733	0.052151	0.7693	−116.914447	−116.948211	9.9091279	0.0215
ts3	−117.1969821	0.056003	0.7594	−116.930143	−116.963917	2.4660921	0.0147
ts4	−117.1932227	0.060357	0.757	−116.924861	−116.959011	8.1135176	0.0157
ts5	−117.1911153	0.056981	0.7614	−116.928428	−116.962469	3.8720777	0.0148
ts6	−117.1998667	0.059239	0.7707	−116.93527	−116.968725	1.618669	0.0177
ts7	−117.2128253	0.06359	0.7972	−116.948111	−116.981881	−4.0435052	0.0299
ts8	−117.1938428	0.056306	0.7581	−116.931017	−116.965006	1.8798399	0.0137
ts9	−117.1880951	0.053026	0.7601	−116.918734	−116.952665	7.590298	0.0175
ts10	−117.2711312	0.063991	0.7537	−117.008046	−117.041408	−40.968795	0.0115
ts11	−117.1291041	0.060359	0.7946	−116.8599398	−116.8938094	49.15124714	0.0381
ts12	−117.183114	0.058918	0.7567	−116.91773	−116.951852	11.714659	0.0118
ts13	−117.1560805	0.056575	0.7576	−116.895997	−116.929964	24.047055	0.0114
ts14	−117.1887157	0.060086	0.7644	−116.925651	−116.95929	7.990005	0.0153
ts15	−117.251638	0.063639	0.7599	−116.987127	−117.020721	−28.308672	0.0141

2. The collisionless limit of the multiple-well ME. As the name implies, this equation is simply the p → 0 limit of the above ME. However, in the limiting case we can solve the problem in both one and two dimensions. In the latter case *E* and *J*, where *J* is the total angular momentum quantum number, are the independent variables. In the present investigation, *J* conservation was never a significant issue. Nevertheless, all the results reported in this article are from two-dimensional calculations.

3. The single-well (multiple-product) master equation describing irreversible dissociation. As above, we can compute rate coefficients using this method both in one and two dimensions with *E* or *E* and *J* as the independent variables. The two-dimensional calculations are facilitated by an approximation to the collision kernel in the ME.[16] All the results reported are from the two-dimensional ME. For the pressures and temperatures of interest to us here, angular momentum effects are negligible.

There are two types of transition probabilities in the master equation, collisional and reactive. For the present work we employ Lennard-Jones collision rates and approximate the energy transfer function using the single-exponential-down model with $\langle \Delta E_d \rangle = 80(T/300\ \mathrm{K})^{0.7}\ \mathrm{cm}^{-1}$. This energy transfer model is used whether the collider is argon or helium, the only 2 bath gases considered in this work. The energy transfer function is also assumed to be independent of energy, angular momentum, and isomeric form of the complex. Probably none of these approximations are accurate, not even the exponential form of the energy transfer function.[13] However, thermal rate coefficients are only weakly dependent on these details, and knowledge of them is severely lacking in general.

Microcanonical, *J*-resolved RRKM rate coefficients, $k(E,J)$, are calculated in this work using variational transition-state theory for the association/dissociation reactions and conventional transition-state theory for the isomerizations and abstractions. In the variational approach, the dividing surface is chosen from a one-parameter family of surfaces perpendicular to the minimum energy path; there is one dividing surface for every *E*, *J* combination, and the minimum-flux condition is used to establish the position of the surface and the corresponding $k(E,J)$. For the one-dimensional ME calculations the $k(E)$ functions are constructed directly from the $k(E,J)$'s to preserve the accuracy of the *J*-resolved rate coefficients as much as possible. Tunneling and nonclassical reflection (both of which are automatically included in the quantum transition probabilities) are included in the analysis one-dimensionally by assuming that the potential along the minimum-energy path can be approximated by an asymmetric Eckart function.

The electronic-structure calculations were done with Gaussian 03[47] and MOLPRO.[48] The RRKM and master-equation calculations were performed with VARIFLEX.[49] Aspects of the methodology used in VARIFLEX germane to the present investigation are described in previous papers.[9−13,16,50]

Potential Energy Surface

The results of the electronic structure calculations are given in Table 1, and the PES is depicted diagrammatically in Figure 1. Three saddlepoints (transition states) are not shown in the figure—ts2 is the transition state for H abstracting a hydrogen atom from allene, ts9 is a similar transition state for H abstracting a hydrogen atom from propyne to form propargyl plus H_2, and ts10 is the transition state for internal rotation about the C−C bond in allyl. The table shows that neither spin contamination in the DFT calculations nor multireference character in the QCISD(T) wave functions is an issue. The only structures that have T1 (or Q1) diagnostics of the order of 0.03 or larger are ts7 and ts11, and neither of these transition states plays a significant role in the rate coefficient determinations.

Although somewhat more accurate and more complete than previous investigations of the C_3H_5 potential, the present results are not much different from those obtained in the previous work. However, two points of kinetic significance have not been appreciated fully in the past. The first is that the threshold energy

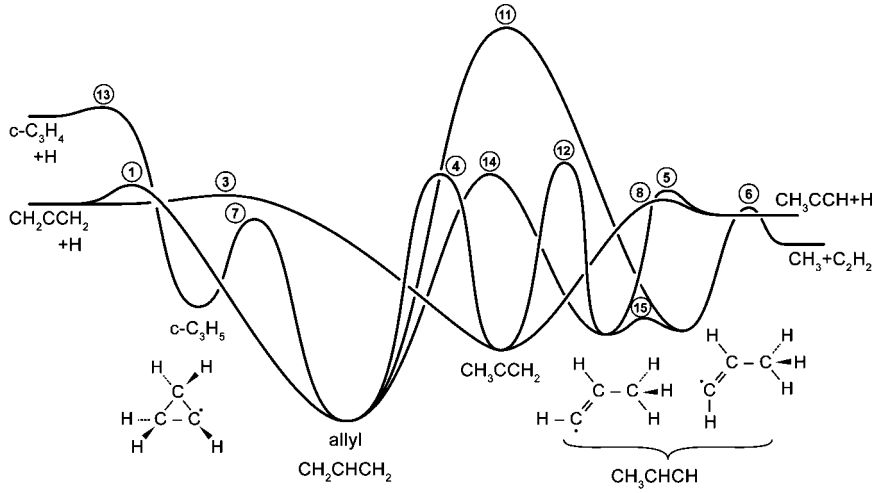

Figure 1. Potential energy diagram for the C_3H_5 potential.

for allyl isomerizing to cyclopropyl is smaller than that for it dissociating to $C_3H_4a + H$. Nevertheless, c-C_3H_5 plays no significant role in the kinetics unless one is specifically interested in it as a reactant or product. We confirmed this result by direct calculation, but ultimately it is true because c-C_3H_5 is inconsequential in both its microcanonical (appropriate at low pressure) and canonical (appropriate at high pressure) equilibria with allyl.

Another, more significant aspect of the potential that appears to have been universally ignored in the past is that 1-propenyl (CH_3CHCH) exists in 2 isomeric forms CH_3CHCH (cis) and CH_3CHCH (trans). CH_3CHCH (cis), where the HCCH is in its cis configuration, is more stable than CH_3CHCH (trans) by about 1/2 kcal/mol. The 2 are separated by an in-plane barrier of ~4 kcal/mol in the exothermic direction. It is the cis form that is connected to $C_3H_4p + H$, but the trans configuration is connected to $CH_3 + C_2H_2$. In the vast majority of our master equation calculations we assumed the two isomers to be distinct species, only adding their contributions to the rate coefficients at the end. However, in some calculations we combined the two into one "superspecies" from the outset by adding the state densities, etc. The same rate coefficients were obtained in either case. In any event, at low pressures the increased lifetimes of the two-well system (over those of only one well) can have a significant effect on the rate coefficients, particularly those for stabilization. Unlike the existence of c-C_3H_5, this effect in general cannot be ignored.

The transition states governing isomerizations among the principal radicals (allyl, 1-propenyl, and 2-propenyl), namely ts4, ts11, ts12, and ts14, are all high and tight. For most applications they can be viewed as impenetrable (confirmed by direct calculation). In light of the previous discussion, many problems can be reduced to simple one-well problems. Although we exploited this property of the PES in a few instances, the majority of the calculations were performed with the full potential.

Our own tests[51] indicate that the electronic-structure methods described above lead to barrier heights that are accurate to about 2 kcal/mol; minima are somewhat more accurate. Table 2 shows the modifications to the computed barrier heights that are required to obtain the level of agreement with experiment shown in the remainder of this article. Except that for ts6, all these adjustments are less than 2 kcal/mol, and the accuracy of the experiments on which we based our change to ts6 has been questioned in the past.[22]

TABLE 2: Modifications to Transition-State Energies (kcal/mol)

ts1	ts3	ts5	ts6	ts8
−1.49	−0.66	−0.63	−2.34	−1.43

Allyl Dissociation and H + Allene → Products

Allyl dissociation and its reverse, $H + C_3H_4a \rightleftarrows CH_2CHCH_2$ are governed by ts1. Determining these rate coefficients is straightforward, but the reaction has some interesting features. The structure of ts1 is shown in Figure 2a. The incoming (if viewed from the association perspective) hydrogen atom can lie in any one of 4 equivalent CCH planes. The normal-mode analysis of ts1 suggests that the mode with the lowest frequency, 139 cm^{-1}, should be treated as an internal rotation in which the H atom rotates almost freely about the central allene core. A scan of this rotation shows that the hindering potential has a barrier of only 125 cm^{-1}; i.e., there are four equivalent minima, each of which is separated from one on each side of it by a barrier of this height. We adopted this characterization of this degree of freedom in the rate-coefficient calculations.

As the H atom moves inward along the IRC (minimum energy path) toward the central carbon atom, the hindrance barrier corresponding to this low-frequency motion first increases up to about 204 cm^{-1}, then it decreases, ultimately to zero. There follows then a region where the potential slopes down away from the IRC in this degree of freedom, as indicated by imaginary harmonic frequencies. As the IRC is traversed inward, the motion corresponding to this normal mode acquires a twist of one CH_2 relative to the other. The terminal point of the IRC turns out not to be the allyl well, as one might normally

Figure 2. (a) Transition state for hydrogen atom adding to the central carbon of allene and (b) the terminal point of the IRC moving inward.

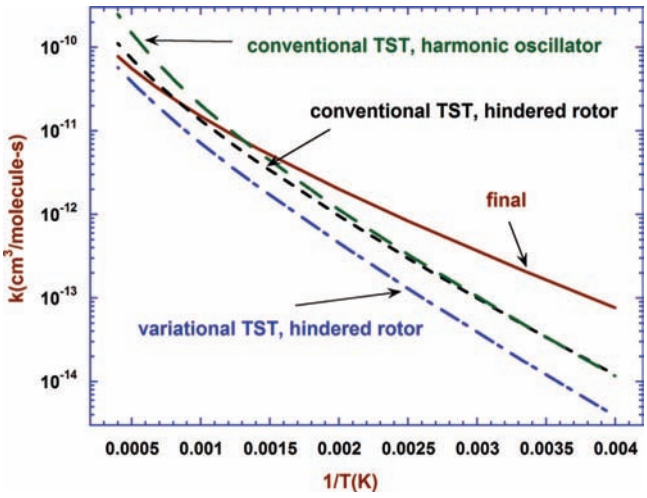

Figure 3. High-pressure-limit rate coefficients for H + $C_3H_4a \rightarrow CH_2CHCH_2$ with various approximations.

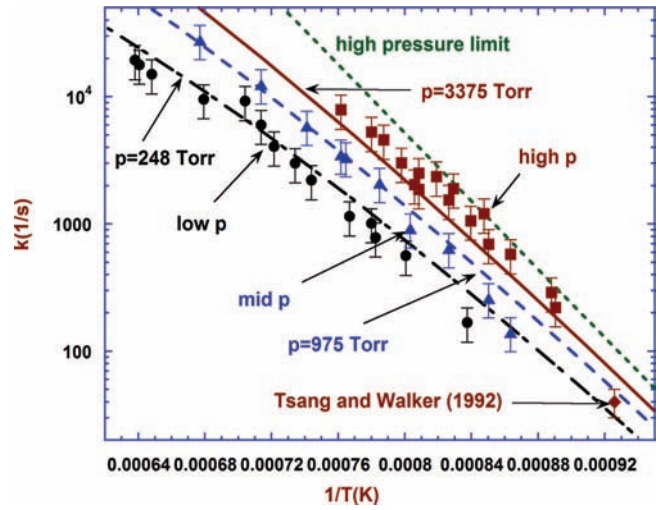

Figure 4. Rate coefficient for the dissociation of allyl. The experimental data points are from Fernandes et al.[18]

expect—such a minimum energy path is forbidden by symmetry. The actual terminal point is shown in Figure 2b. It corresponds to the transition state for allyl rotating into itself through a torsional motion about one of the C−C bonds—the low frequency mode described above becomes the reaction coordinate for this transformation.

Figure 3 shows a comparison of various approximations used in calculating the high-pressure-limit (HPL) association rate coefficient for H + $C_3H_4a \rightarrow CH_2CHCH_2$. Using conventional transition-state theory, going from a harmonic-oscillator approximation for the ts1 normal mode described above to the hindered-rotor treatment reduces the rate coefficient by a factor of 2.5 at 2500 K. The difference is negligible at low temperatures. This reduction in the rate coefficient at high T occurs because the hindered-rotor treatment restricts the motion of the hydrogen atom to a closed loop (circle), whereas the low-frequency oscillator treatment allows a very large-amplitude motion at high energies. The sums of states and partition functions are modified accordingly, thus reducing the entropy of the transition state at high temperatures when the hindered-rotor treatment is employed.

Retaining the hindered-rotor approximation and switching from conventional TST to variational TST results in another reduction in the rate coefficient, as shown in Figure 3. Actually, almost none of the difference between the 2 curves in the figure is due to variational effects. The reduction in rate coefficient arises because the QCISD(T) single-point energies calculated along the IRC result in a barrier (the IRC_{max}) that does not coincide with the original B3LYP saddlepoint. This larger barrier, not variational effects, produces the smaller rate coefficients. Limited testing[52] suggests that the procedure adopted here is superior to one in which the original saddlepoint is retained; i.e., the former gives results that are more consistent with those obtained when the same high-level quantum chemistry is used for both the search and the energies. In the present case, the IRC_{max} is 0.48 kcal/mol higher than the original saddlepoint, but the barrier was reduced by 1.49 kcal/mol to improve agreement with experiment, as indicated in Figure 3. This type of behavior was observed throughout this work; it suggests that one may benefit from canceling errors, at least in some cases, by retaining the original saddlepoint.

Figure 4 compares the present predictions of the rate coefficient for allyl dissociation with the shock tube experiments of Fernandes et al.[18] The experiments were performed at pressures that clustered around the values used in the calculations. Also shown on the plot is the experimental result of Tsang and Walker,[30] which was obtained at pressures between 2 and 7 atm. Overall, the agreement between theory and experiment is excellent. The present theoretical results differ from those of Fernandes et al. in a number of ways, perhaps most importantly in the hindered-rotor treatment of the low-frequency normal mode discussed above.

Figure 5 compares our predictions for the H + C_3H_4a rate coefficient with the low-temperature experiments of Wagner and Zellner,[27] conducted at pressures between 1 and 20 Torr. The formation of allyl is not the dominant product channel of this reaction. Theory and experiment agree that H adding to the terminal carbon in allene, leading to 2-propenyl and H + C_3H_4p, is faster. Overall, the agreement between theory and experiment is satisfactory. Indeed, both indicate that the rate coefficients are relatively independent of pressure in the range of the experimental investigation. The big discrepancy is for the allyl channel, where the theoretical predictions are roughly a factor of 4 larger than the experimental results. In agreement with Tsang and Walker, we find it difficult to reconcile these experiments with the high temperature dissociation experiments and the known thermochemistry. The relatively large corrections in their rate coefficients made by Wagner and Zellner for secondary reactions may be symptomatic of large errors in the final results.

Reaction Between Hydrogen Atoms and Propyne

The H + C_3H_4p reaction has been studied in the laboratory several times in the past. However, we want to focus our attention here on the two sets of experiments that appear to be most reliable and illuminating, those of Whytock et al.[24] and those of Bentz et al.[21] The former were conducted at low temperatures, 215 K $\leq T \leq$ 460 K, in the pressure range, 5 Torr $\leq p \leq$ 600 Torr, whereas the latter were performed at higher temperatures, 1200 K $\leq T \leq$ 1400 K, and at pressures roughly between 1.3 and 4.0 atm.

The barrier for H adding to the terminal (CH) carbon in propyne is somewhat smaller than that for adding to the central carbon. Consequently, at low temperatures the reaction is dominated by stabilization to form CH_3CCH_2 (2-propenyl), as one would expect from Figure 1, even though the bimolecular channels, C_2H_2 + CH_3 and C_3H_4a + H, are not negligible even

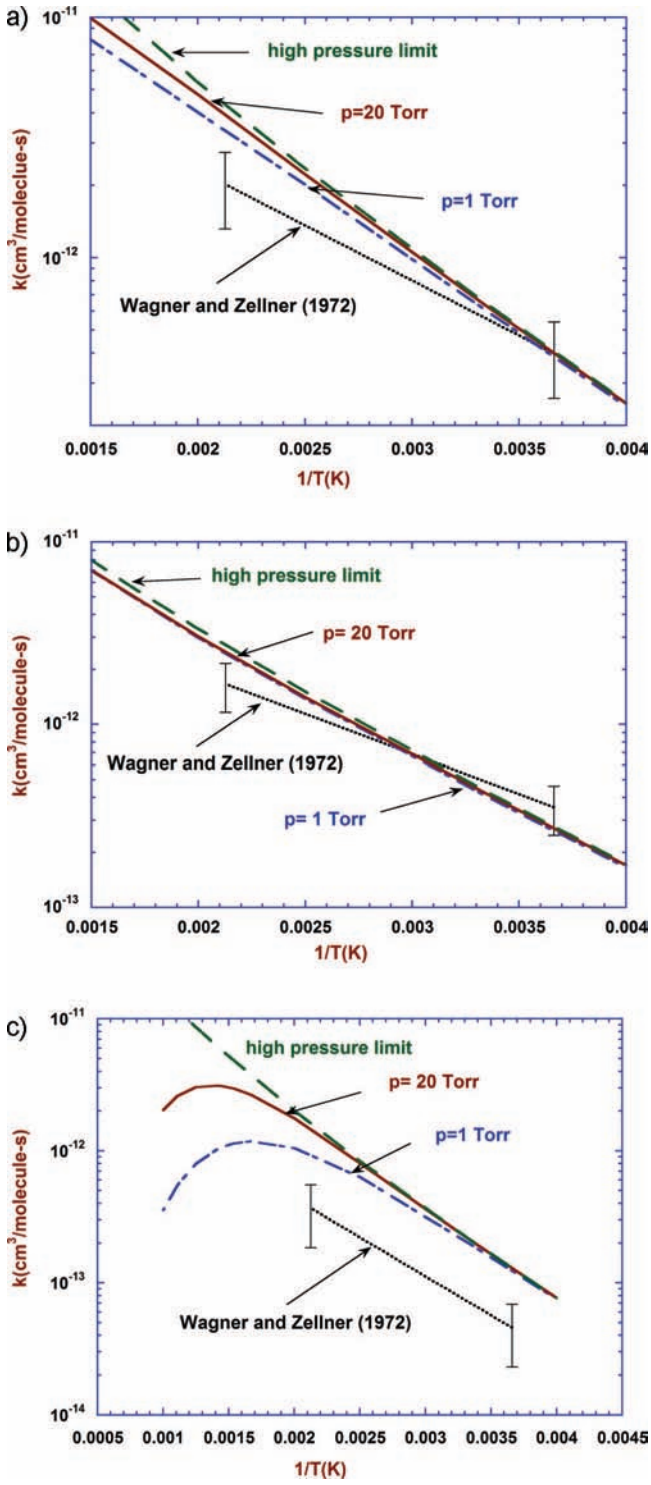

Figure 5. H + C_3H_4a → products rate coefficient: (a) total rate coefficient; (b) H adding to the terminal carbon; (c) H adding to the central carbon.

at the highest pressure studied by Whytock et al. Thus the total rate coefficient depends significantly on the pressure. In Figure 6 we compare our predictions of the HPL rate coefficient, $k_\infty(T)$, with the experimental determinations of Whytock et al. In Figures 7a,b we compare our predictions of the pressure dependence of the rate coefficient for H + C_3H_4p → products with their results for the two highest temperatures they investigated, 363 and 460 K; at these temperatures variation of the rate coefficient with pressure was the largest. The agreement between theory and experiment is excellent.

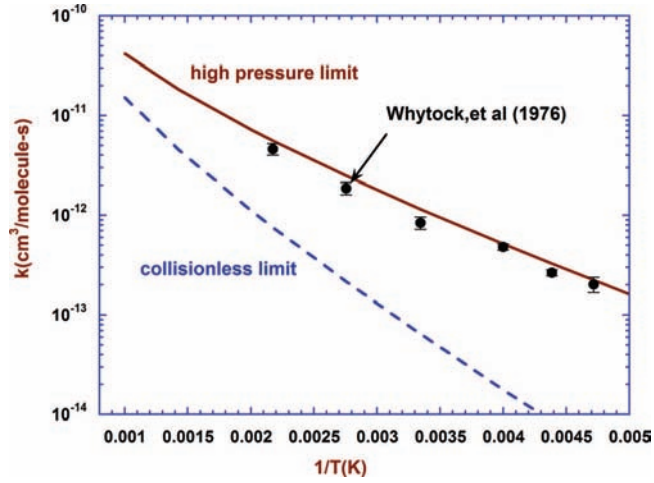

Figure 6. High-pressure limit of the H + C_3H_4p rate coefficient at low temperature.

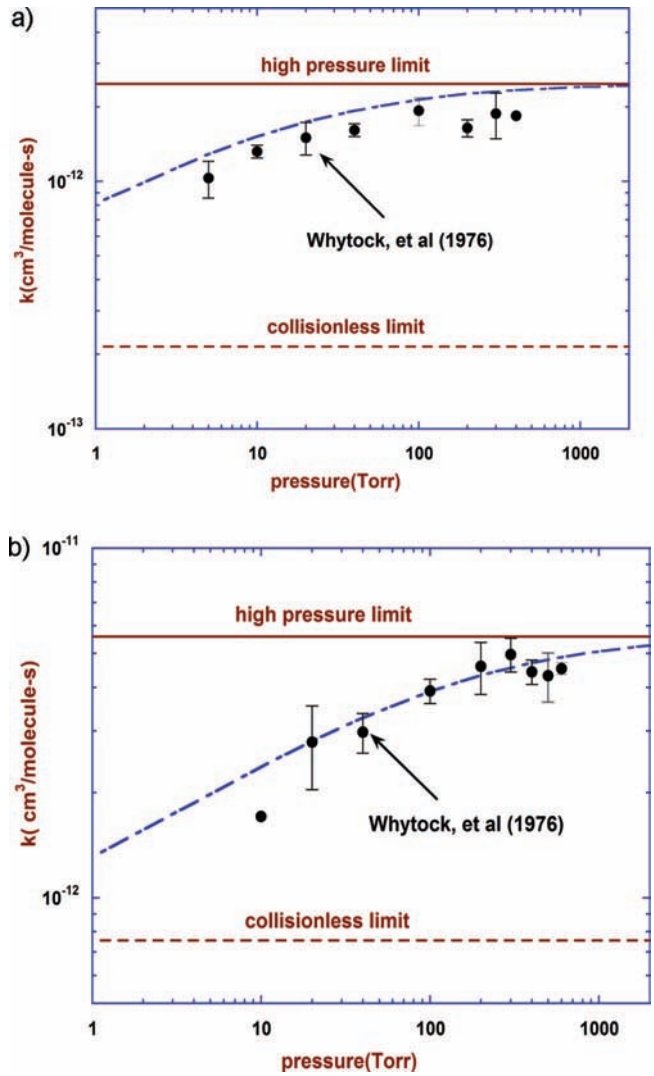

Figure 7. Pressure dependence of the H + C_3H_4p rate coefficient: (a) T = 363 K; (b) T = 460 K.

Interestingly, the collisionless-limit (or zero-pressure) rate coefficient at the temperatures studied by Whytock et al. is dominated by the C_3H_4a + H product channel, even though these products are slightly endothermic. For example, at 250 K 74% of k_0 is due to C_3H_4a + H and 26% due to C_2H_2 +CH_3 with about a 0.1% contribution from the abstraction. However,

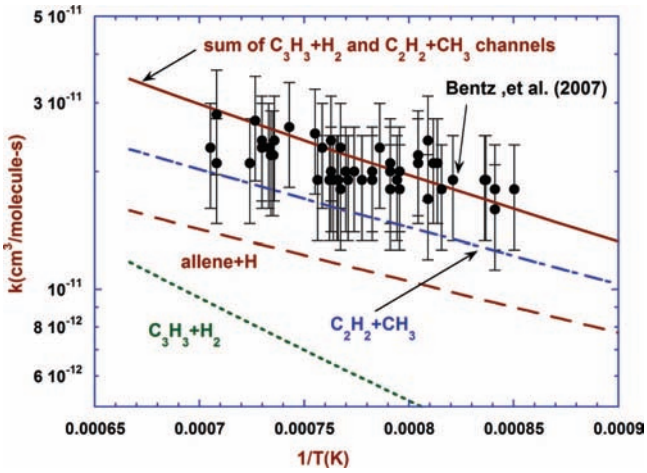

Figure 8. High temperature rate coefficients for H + C_3H_4p → products.

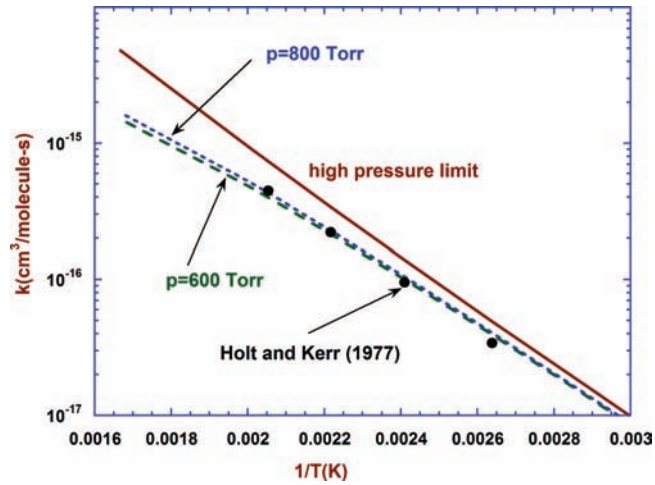

Figure 9. High pressure, low temperature rate coefficient for CH_3 + C_2H_2 → products.

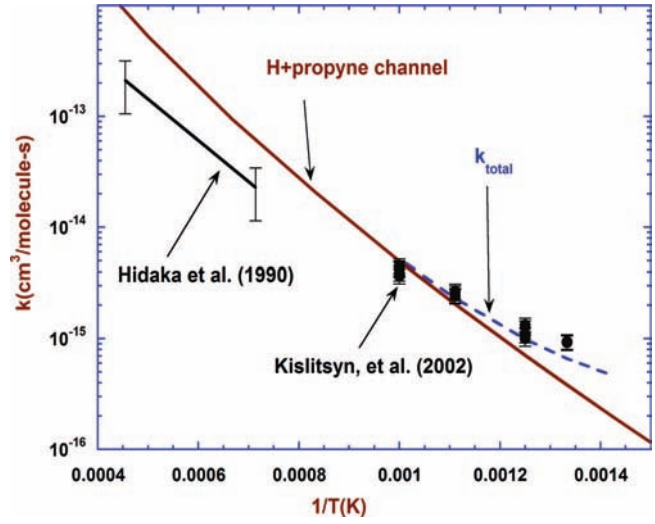

Figure 10. High temperature rate coefficient for CH_3 + C_2H_2 → products.

this product distribution varies with temperature. Both the C_2H_2 + CH_3 and C_3H_3 + H_2 channels rise more rapidly with T than does C_3H_4a + H. Between 700 and 2000 K the C_2H_2 + CH_3 products are dominant, and above 2000 K the abstraction takes over.

In Figure 8 we compare our results with the shock-tube experiments of Bentz et al.[21] These comparisons require a little bit of explanation. The observable in these experiments is the H-atom concentration. Consequently, the reaction C_3H_4p + H → C_3H_4a + H is invisible to the experiment, because it does not produce a change in the concentration of hydrogen atoms. Also, our calculations indicate that the stabilization reaction, H + C_3H_4p ⇄ CH_3CCH_2, is not completely negligible at the lower end of the temperature range; i.e., its rate coefficient is not insignificant compared to those of other channels. However, under the conditions of the experiments equilibrium heavily favors the H + C_3H_4p reactants, so that this channel is also invisible to the experiments. The only two channels that contribute to the rate coefficients measured by Bentz et al. are C_3H_3 + H_2 and C_2H_2 + CH_3, both of whose rate coefficients are essentially independent of pressure under the conditions of the experiments. When we add these two rate coefficients together, the agreement with experiment is remarkably good, even better than the results of the analysis in the Bentz et al. article.

CH_3 + C_2H_2 Reaction

In studying the reaction between methyl and acetylene we focus our attention on the experiments of Holt and Kerr[25] and Kislitsyn et al.[19] Both investigations were conducted at temperatures below 1000 K. Holt and Kerr's experiments are at pressures high enough that the rate coefficient for the reaction CH_3 + C_2H_2 → CH_3CHCH is very close to its high-pressure limiting value. Consequently, their results can be used to test and correct our barrier height for ts6. Diau and Lin[22] studied in detail the experiments of Mandelcorn and Steacie,[32] Garcia Dominquez and Trotman-Dickinson,[31] and Holt and Kerr[25] in an effort to re-evaluate rate coefficients derived from these experiments for the CH_3 + C_2H_2 reaction. They concluded that the Holt and Kerr experiments were not sensitive enough to the rate coefficient in question to deduce an accurate value. Nevertheless, the Holt and Kerr rate coefficients were found to be consistent with the values Diau and Lin deduced from the other experiments and with their own theoretical value. Therefore, we conclude that they are the best available test of our barrier height. The Kislitsyn experiments, which are the only ones considered in this investigation to use helium rather than argon as the diluent, represent the only direct measurements of the CH_3 + C_2H_2 rate coefficient to date. As such, they clearly warrant our attention.

In Figure 9 we compare our theoretical results (after the barrier-height adjustment of Table 2) with the experimental rate coefficients of Holt and Kerr. The two pressures for which calculated rate coefficients are plotted in Figure 9 (600 and 800 Torr) bound the pressures investigated in the experiments. At these pressures the rate coefficient is very close to its high-pressure limit, and as a result it does not depend very much on the pressure, as can be seen from the plot. Modifying only a barrier height and thus obtaining agreement with experiment for both magnitude and temperature dependence of the rate coefficients is usually an indication that both theory and experiment are reliable.

Figure 10 compares our predictions for the CH_3 + C_2H_2 rate coefficients with the measurements of Kislitsyn et al.[19] Under the conditions of these experiments the principal product channel is C_3H_4p + H, but Kislitsyn et al. voice concern in their article that their lower-temperature experiments may also have contributions from the stabilization reaction forming 1-propenyl. Both our predictions for the C_3H_4p + H channel and the total

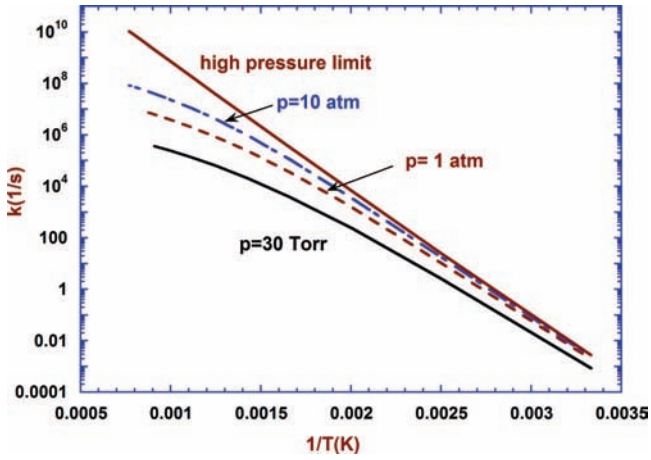

Figure 11. Rate coefficient for the isomerization of cyclopropyl to allyl. Note that 1 atm = 760 Torr.

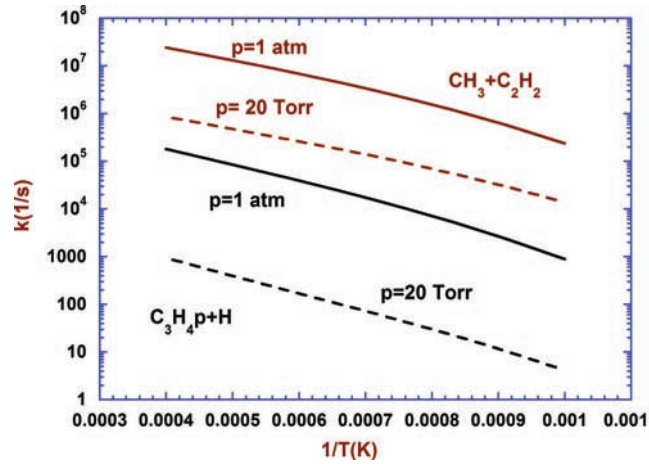

Figure 12. Rate coefficients for the dissociation of 1-propenyl. Note that 1 atm = 760 Torr.

rate coefficient are shown in Figure 10. As can be seen from the plot, the k_{total} result is in better agreement with the experiment. However, under the conditions of these experiments, the equilibrium of the $CH_3 + C_2H_2 \rightleftarrows CH_3CHCH$ reaction favors the reactants. This means that, for the stabilization reaction to contribute to the loss of CH_3 in the experiment (the means by which the rate coefficient was determined), there would have to be a fast secondary reaction removing CH_3CHCH. Such a reaction is plausible, and one cannot rule out the possibility that the Kislitsyn results are a measure of k_{total}.

Also shown in Figure 10 is the experimental determination of Hidaka et al.,[20] which was derived from modeling shock tube experiments on methane pyrolysis. The theoretical analysis of Diau et al.[23] resulted in good agreement with Hidaka's experiment, and Kislitsyn et al. forced their theory to agree with Hidaka. However, it appears now that these experiments are simply in error. Hidaka's experiments and those of Bentz et al. on $C_3H_4p + H$, discussed in the last section, are largely governed by the same transition state, ts5, and were conducted in temperature ranges that almost overlap. It is not possible to predict both results with any realistic model. The present theoretical analysis is able to account for the results of the two direct measurements, those of Bentz et al. and Kislitsyn et al. without difficulty.

Isomerization of Cyclopropyl to Allyl

Cyclopropyl (c-C_3H_5) is a minor player in the chemistry of the C_3H_5 potential. However, its isomerization/dissociation is part of the story, and we shall consider it briefly. The experimental data on cyclopropyl isomerization is very old and apparently not very accurate.[53] Consequently, it is not of much use to us in testing our theoretical model, and we shall forego theory/experiment comparisons. That leaves us to present our theoretical results for the rate coefficient of c-$C_3H_5 \rightleftarrows CH_2CHCH_2$ in Figure 11. The second most important channel for c-C_3H_5 isomerization/dissociation is the "well-skipping" dissociation[9,54,55] to form $C_3H_4a + H$, but this rate coefficient only comes within 2 orders of magnitude of the isomerization at the very highest temperatures shown on the plot.

Cyclopropyl exhibits a common feature of shallow wells on complex potentials: its thermal isomerization to form allyl equilibrates on vibrational−rotational time scales at relatively low temperatures.[9,11−13] In the present case this occurs between 1200 and 1400 K as the pressure increases from 30 Torr to 10 atm, thus defining the upper limits of the curves in Figure 11. Beyond this point, the rate coefficient ceases to be a useful, perhaps even meaningful, concept. At higher temperature the two isomers behave kinetically as if they were one species.[9,11−13]

Thermal Dissociation of Weakly Bound Free Radicals: 1-Propenyl, 2-Propenyl, and Allyl

The high-temperature dissociation rate coefficients for 1-propenyl and 2-propenyl are shown in Figures 12 and 13 (the dissociation of allyl was discussed above). Whereas allyl has only one significant dissociation channel ($C_3H_4a + H$), 1-propenyl and 2-propenyl each have two: $CH_3 + C_2H_2$ and $C_3H_4p + H$ for 1-propenyl and $C_3H_4p + H$ and $C_3H_4a + H$ for 2-propenyl. For both radicals the lower-energy product channel dominates at both pressures shown in the plots, as it does all the way up to the high-pressure limit in the present cases. The ratio of the rate coefficient of the dominant channel to that of the secondary channel increases with deceasing pressure, as expected. This behavior occurs because dissociation through the low-energy channel increasingly dominates over collisional activation as the pressure is reduced, allowing the low-energy channel to "rob" flux from the high-energy products.

Allyl, 1-propenyl, and 2-propenyl are all weakly bound free radicals. To be specific, we define a weakly bound free radical to be one whose primary dissociation products are a stable molecule and another radical. The radical in the dissociation products is frequently, but not always, a hydrogen atom. In the present case, 1-propenyl can dissociate into either $CH_3 + C_2H_2$ or $C_3H_4p + H$, both of which are radical + molecule channels. Such radicals have weak bonds and thus dissociate rapidly at high temperatures. This rapid dissociation leads to coupling between internal-energy relaxation and dissociation. As a consequence of this coupling, some dissociation occurs as part of the vibrational−rotational relaxation process, thus compromising the utility of the rate-coefficient (phenomenological) description, at least to some extent. Allyl, because of its resonant electronic structure, has a bond energy of about 55 kcal/mol, making it one of the most stable of the weakly bound free radicals. Consequently, allyl's behavior at high temperature is of particular interest as a limiting case.

In Figure 14 we have plotted the nonequilibrium factors, f_{ne}, for the three radical dissociations. This parameter is a function of the steady-state population distribution of the dissociating radical. It is defined mathematically and discussed extensively in previous publications.[9,15] We content ourselves here with

TABLE 3: Thermal Rate Coefficients Represented as Modified Arrhenius Functions

pressure (Torr)	A_1 (cm^3/(molecule s))	n_1	E_{0_1} (cal/mol)	A_2 (cm^3/(molecule s))	n_2	E_{0_2} (cal/mol)
			H + Allene ⇄ Allyl			
1	0.367×10^{38}	−15.25	20076	0.465×10^{15}	−8.67	8035
30	0.206×10^{29}	−12.02	17839	0.115×10^{14}	−8.19	7462
760	0.776×10^{28}	−11.45	21340	0.551×10^{7}	−5.78	6913
7600	0.622×10^{25}	−10.27	22511	380	−4.32	6163
76000	0.703×10^{20}	−8.61	22522	0.728×10^{-2}	−2.71	5187
∞	6.79×10^{-14}	0.970	2609			
			H + Allene ⇄ H + Propyne			
0	4.06×10^{-14}	1.04	2159			
1	1.41×10^{-13}	0.89	2503			
30	2.45×10^{-11}	0.26	4103			
760	4.11×10^{-9}	−0.33	6436			
7600	39.06	−3.23	13165	0.289×10^{-16}	1.98	4521
76000	1.70	−2.67	15552	0.769×10^{-19}	2.62	4466
			H + Allene ⇄ CH_3 + C_2H_2			
0	6.21×10^{-23}	3.35	57.75			
1	2.05×10^{-16}	1.53	4737			
30	4.52×10^{-15}	1.20	6834			
760	0.210×10^{-3}	−1.83	15003	0.204×10^{-19}	2.68	6335
7600	0.279×10^{-7}	−0.60	14754	0.549×10^{-15}	1.14	8886
76000	0.228×10^{-6}	−0.79	17603	0.212×10^{-17}	1.71	9774
			H + Allene ⇄ CH_3CCH_2			
1	0.107×10^{80}	−27.51	51768	0.182×10^{31}	−14.29	10809
30	0.258×10^{30}	−13.10	14472	0.164×10^{22}	−11.21	8212
760	0.315×10^{30}	−12.59	16726	0.466×10^{17}	−9.42	7850
7600	0.132×10^{29}	−11.82	18286	0.431×10^{12}	−7.57	7147
76000	0.699×10^{29}	−11.64	22262	0.164×10^{7}	−5.53	6581
∞	1.056×10^{-14}	1.26	2051			
			H + Propyne ⇄ CH_3CCH_2			
1	0.147×10^{29}	−13.04	12325	0.327×10^{23}	−11.91	7456
30	0.527×10^{29}	−12.69	14226	0.430×10^{22}	−11.23	8046
760	0.476×10^{30}	−12.51	16853	0.115×10^{17}	- 9.11	7458
7600	0.158×10^{29}	−11.74	18331	0.113×10^{12}	−7.29	6722
76000	0.749×10^{29}	−11.58	22207	0.938×10^{6}	−5.39	6150
∞	1.365×10^{-13}	0.940	1926			
			H + Propyne ⇄ CH_3CHCH			
1	-0.284×10^{16}	−10.47	7722	0.247×10^{15}	−10.11	7458
30	0.561×10^{26}	−12.75	14072	0.495×10^{20}	−11.43	8736
760	0.227×10^{28}	−12.55	15428	0.955×10^{16}	−9.51	8772
7600	0.644×10^{27}	−11.90	16915	0.719×10^{17}	−9.60	9401
76000	0.360×10^{26}	−11.10	18746	0.571×10^{11}	−7.36	8558
∞	2.92×10^{-14}	1.09	3949			
			H + Propyne ⇄ CH_3 + C_2H_2			
0	3.52×10^{-14}	1.06	3945			
1	4.06×10^{-14}	1.04	3980			
30	6.46×10^{-14}	0.989	4114			
760	5.74×10^{-12}	0.442	5463			
7600	2.86×10^{-10}	−0.01	7134			
76000	-0.123×10^{8}	−5.54	12108	0.316×10^{-8}	−0.290	8306
			CH_3 + C_2H_2⇄ CH_3CHCH			
1	-0.824×10^{103}	−37.53	42751	0.295×10^{18}	−10.40	13647
30	-0.113×10^{26}	−12.27	16642	0.253×10^{21}	−10.73	15256
760	0.198×10^{21}	−10.19	18728	0.141×10^{13}	−8.43	12356
7600	0.999×10^{20}	−9.74	20561	0.504×10^{9}	−7.01	12357
76000	0.235×10^{19}	−8.91	22235	2.814×10^{3}	−5.07	11690
∞	2.23×10^{-19}	2.49	7105			

pressure (Torr)	A_1 (1/s)	n_1	E_{0_1} (cal/mol)
	c-C_3H_5 ⇄ CH_2CHCH_2		
30	9.25×10^{34}	−8.047	24861
760	5.16×10^{35}	−7.784	26318
7600	1.00×10^{34}	−6.925	26806
∞	2.19×10^{10}	1.054	21337

A_1 (cm^3/molecule-s)	n_1	E_{0_1} (cal/mol)
	H + Propyne ⇄ C_3H_3 + H_2	
5.93×10^{-20}	2.825	4821

A_1 (cm^3/(molecule s))	n_1	E_{0_1} (cal/mol)
	H + Allene ⇄ C_3H_3 + H_2	
1.10×10^{-20}	3.095	5522

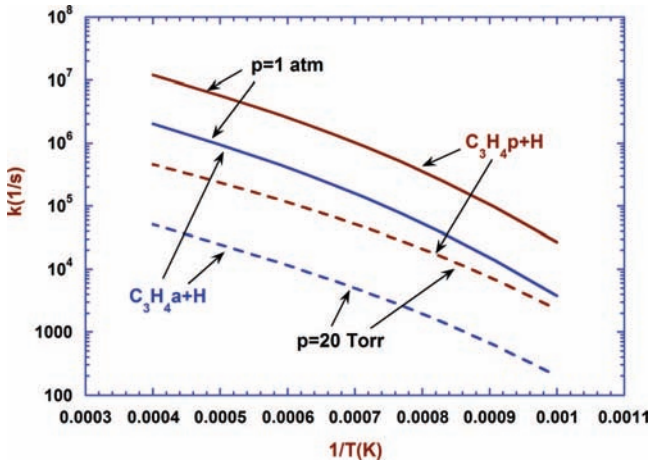

Figure 13. Rate coefficients for the dissociation of 2-propenyl. Note that 1 atm = 760 Torr.

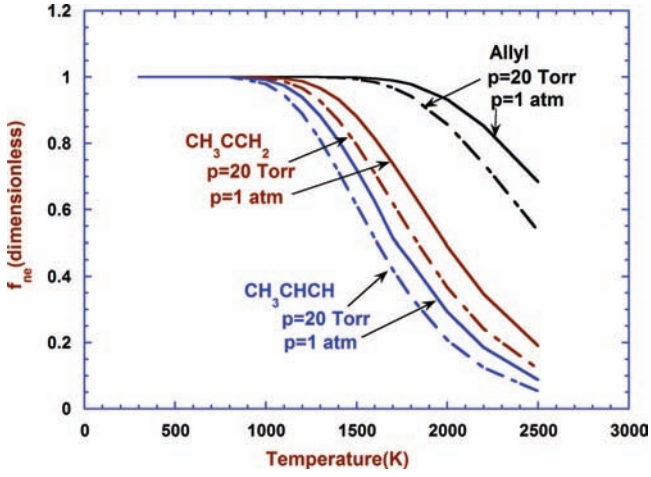

Figure 14. Nonequilibrium factors for the dissociations of allyl, 1-propenyl, and 2-propenyl. Note that 1 atm = 760 Torr.

discussing its physical interpretation. If the population distribution of the dissociating molecule is Boltzmann, $f_{ne} = 1$. As long as the perturbation of the equilibrium population distribution induced by dissociation is restricted to the high-energy tail of the distribution, f_{ne} will be equal to unity to a high degree of accuracy (usually many significant digits). This is the case for stable molecules even at high temperature. However, when chemical reaction begins to perturb the populations of states that are highly populated at equilibrium, f_{ne} will begin to drop below unity. This occurs in all the calculations shown in Figure 14.

As one would expect, $(1 - f_{ne})$ increases with decreasing pressure and with decreasing bond energy, or dissociation threshold. For allyl, f_{ne} drops below 0.9 only at a temperature of about 2000 K, even at 20 Torr. However, for the other two radicals, f_{ne} deviates markedly from unity at much lower temperatures. This deviation indicates that a phenomenological description of these reactions (i.e., in terms of thermal rate coefficients) is not completely satisfactory. The issue of how to incorporate these reactions in chemical kinetics models has not yet been completely resolved. It is fortunate that in many such cases the dissociation is so rapid that model predictions are not very sensitive to these rates.

Concluding Remarks

The analysis of the reactions occurring on a C_3H_5 potential described above is a good illustration of the power of the master-equation methods we have developed over the past few years.[9−16] With only modest adjustments to some of the barrier heights we were able to obtain excellent agreement between the theory and a wide range of experimental results. The theoretical rate coefficients should be good enough to characterize the reactions of interest over wide ranges of temperature and pressure. To this end we have fit our rate coefficients to the form,

$$k(T,p) = \sum_{j=1}^{2} A_j(p) T^{n_j(p)} \exp[-E_0^{(j)}(p)/RT] \qquad (7)$$

i.e., the rate coefficient at any pressure is represented as a sum of two modified Arrhenius functions (sometimes one function is sufficient), These results can be used directly in CHEMKIN 4.1[56] or higher, which interpolates log k linearly as a function of log p at any temperature. The Troe form for $k(T,P)$, an alternative to the present representation, is generally a good characterization of the rate coefficient only for the barrierless, single-well combination of two radicals. The representation used here is considerably more flexible. Our results with argon as the bath gas are given in Table 3. Rate coefficients for reverse reactions can be obtained from detailed balance. Except for the c-$C_3H_5 \rightleftarrows CH_2CHCH_2$ reaction, the fits are accurate in the temperature range, 250 K ≤ T ≤ 2500 K. For the cyclopropyl isomerization the rate coefficients are accurate roughly between 300 and 1200 K.

Acknowledgment. This work was supported by the United States Department of Energy, Office of Basic Energy Sciences, Division of Chemical Sciences, Geosciences, and Biosciences. Sandia is a multiprogram laboratory operated by Sandia Corporation, a Lockheed Martin Co., for the United States Department of Energy's National Nuclear Security Administration under contract DE-AC04-94A185000. The work at Argonne was supported under contract no. DE-AC02-06CH11357.

References and Notes

(1) Miller, J. A.; Pilling, M. J.; Troe, J. *Proc. Combust. Inst.* **2005**, *30*, 43–88.
(2) Miller, J. A. *Proc. Combust. Inst.* **1996**, *26*, 461–480.
(3) Miller, J. A. *Faraday Discuss.* **2001**, *119*, 461–475.
(4) Miller, J. A.; Melius, C. F. *Combust. Flame* **1992**, *91*, 21–39.
(5) Richter, H.; Howard, J. B. *Prog. Energy Combust. Sci.* **2000**, *26*, 565–608.
(6) McEnally, C. S.; Pfefferle, L. D.; Atakan, B.; Kohse-Höinghaus, K. *Prog. Energy Combust. Sci.* **2006**, *32*, 247–294.
(7) Glassman, I. *Proc. Combust. Inst.* **1989**, *22*, 295.
(8) Hansen, N.; Miller, J. A.; Taatjes, C. A.; Wang, J.; Cool, T. A.; Law, M. E.; Westmoreland, P. R. *Proc. Combust. Inst.* **2007**, *31*, 1157–1164.
(9) Miller, J. A.; Klippenstein, S. J. *J. Phys. Chem. A* **2006**, *110*, 10528–10544.
(10) Miller, J. A.; Klippenstein, S. J.; Robertson, S. H. *J. Phys. Chem. A* **2000**, *104*, 7525–7536. See also: *J. Phys. Chem. A* **2000**, *104*, 9806.
(11) Klippenstein, S. J.; Miller, J. A. *J. Phys. Chem. A* **2002**, *106*, 9267–9277.
(12) Miller, J. A.; Klippenstein, S. J. *J. Phys. Chem. A* **2003**, *107*, 2680–2692.
(13) Fernandez-Ramos, A.; Miller, J. A.; Klippenstein, S. J.; Truhlar, D. G. *Chem. Rev.* **2006**, *106*, 4518–4584.
(14) Miller, J. A.; Klippenstein, S. J. *J. Phys. Chem. A* **2003**, *107*, 7783–7799.
(15) Miller, J. A.; Klippenstein, S. J. *J. Phys. Chem. A* **2004**, *108*, 8296–8306.
(16) Miller, J. A.; Klippenstein, S. J.; Raffy, C. *J. Phys. Chem. A* **2002**, *106*, 4904–4913.
(17) Davis, S. G.; Law, C. K.; Wang, H. *J. Phys. Chem. A* **1999**, *103*, 5889–5899.
(18) Fernandes, R. X.; Giri, B. R.; Hippler, H.; Kachiani, C.; Striebel, F. *J. Phys. Chem. A* **2005**, *109*, 1063–1070.

(19) Kislitsyn, M. N.; Slagle, I. R.; Knyazev, V. D. *Proc. Combust. Inst.* **2002**, *29*, 1237–1245.
(20) Hidaka, Y.; Nakamura, T.; Tanaka, H.; Inami, K.; Kawano, H. *Int. J. Chem. Kinet.* **1990**, *22*, 701–709.
(21) Bentz, T.; Giri, B. R.; Hippler, H.; Olzmann, M.; Striebel, F.; Szöri, M. *J. Phys. Chem. A* **2007**, *111*, 3812–3818.
(22) Diau, E. W.; Lin, M. C. *Int. J. Chem. Kinet.* **1995**, *27*, 855–866.
(23) Diau, E. W.; Lin, M. C.; Melius, C. F. *J. Chem. Phys.* **1994**, *101*, 3923–3927.
(24) Whytock, D. A.; Payne, W. A.; Stief, L. J. *J. Chem. Phys.* **1976**, *65*, 191–195.
(25) Holt, P. M.; Kerr, J. A. *Int. J. Chem. Kinet.* **1977**, *9*, 185–200.
(26) Hidaka, Y.; Nakamura, T.; Miyauchi, A.; Shiraishi, T.; Kawano, H. *Int. J. Chem. Kinet.* **1989**, *21*, 643–666.
(27) Wagner, H. Gg.; Zellner, R. *Ber. Bunsen-Ges. Phys. Chem.* **1972**, *76*, 667–672.
(28) Wagner, H. Gg.; Zellner, R. *Ber. Bunsen-Ges. Phys. Chem.* **1972**, *76*, 518.
(29) Brown, J. M.; Thrush, B. A. *Trans. Faraday Soc.* **1967**, *63*, 630.
(30) Tsang, W.; Walker, J. A. *J. Phys. Chem.* **1992**, *96*, 8378–8384.
(31) Garcia-Dominguez, J. A.; Trotman-Dickenson, A. F. *J. Chem. Soc.* **1962**, 940–944.
(32) Mandelcorn, L.; Steacie, E. W. R. *Can. J. Chem.* **1954**, *32*, 474.
(33) Wang, B.; Hou, H.; Gu, Y. *J. Chem. Phys.* **2000**, *112*, 8458–8465.
(34) Deyerl, H.-J.; Fischer, I.; Chen, P. *J. Chem. Phys.* **1999**, *110*, 1450–1462.
(35) Fischer, I.; Chen, P. *J. Phys. Chem. A* **2002**, *106*, 4291–4300.
(36) Castiglioni, L.; Bach, A.; Chen, P. *J. Phys. Chem. A* **2005**, *109*, 962–964.
(37) Fan, H.; Pratt, S. T.; Miller, J. A. *J. Chem. Phys.* **2007**, *127*, 144301.
(38) Fan, H.; Pratt, S. T. *J. Chem. Phys.* **2006**, *125*, 144302.
(39) Morton, M. L.; Miller, J. L.; Butler, L. J.; Qi, F. *J. Phys. Chem. A* **2002**, *106*, 10831–10842. See also: *J. Phys. Chem. A* **2002**, *106*, 10965−10967.
(40) Szpunar, D. E.; Morton, M. L.; Butler, L. J.; Regan, P. M. *J. Phys. Chem. B* **2002**, *106*, 8086–8095.
(41) Morton, M. L.; Butler, L. J.; Stephenson, T. A.; Qi, F. *J. Chem. Phys.* **2002**, *116*, 2763–2775.
(42) Mueller, J. A.; Parsons, B. F.; Butler, L. J.; Qi, F.; Sorkhabi, O.; Suits, A. G. *J. Chem. Phys.* **2001**, *114*, 4505–4521.
(43) Mueller, J. A.; Miller, J. L.; Butler, L. J.; Qi, F.; Sorkhabi, O.; Suits, A. G. *J. Phys. Chem. A* **2000**, *104*, 11261–11264.
(44) Stranges, D.; O'Keefe, P.; Scotti, G.; Di Santo, R.; Houston, P. L. *J. Chem. Phys.* **2008**, *128*, 151101.
(45) Martin, J. M. L. *Chem. Phys. Lett.* **1996**, *259*, 669–678.
(46) Feller, D.; Dixon, D. A. *J. Chem. Phys.* **2001**, *115*, 3484–3496.
(47) Frisch, M. J.; Trucks, G. W.; Schlegel, H. B.; Scuseria, G. E.; Robb, M. A.; Cheeseman, J. R.; Montgomery, J. A., Jr.; Vreven, T.; Kudin, K. N.; Burant, J. C.; Millam, J. M.; Iyengar, S. S.; Tomasi, J.; Barone, V.; Mnnucci, B.; Cossi, M.; Scalmani, G.; Rega, N.; Petersson, G. A.; Nakatsuji, H.; Hada, M.; Ehara, M.; Toyota, K.; Fukuda, R.; Hasegawa, J.; Ishida, M.; Nakajima, T.; Honda, O.; Kitao, H.; Nakai, H.; Klene, M.; Li, X.; Knox, J. E.; Hratchian, H. P.; Cross, J. B.; Bakken, V.; Adamo, C.; Jaramillo, J.; Gomperts, R.; Stratmann, R. E.; Yazyev, O.; Austin, A. J.; Cammi, R.; Pomelli, C.; Ochterski, J. W.; Ayala, P. Y.; Morokuma, K.; Voth, G. A.; Salvador, P.; Dannenberg, J. J.; Zakrzewski, V. G.; Dapprich, S.; Daniels, A. D.; Strain, M. C.; Farkas, O.; Malick, D. K.; Rabuck, A. D.; Raghavachari, K.; Foresman, J. B.; Ortiz, J. V.; Cui, Q.; Baboul, A. G.; Clifford, S.; Cioslowski, J.; Stefanov, B. B.; Liu, G.; Liashenko, A.; Piskorz, P.; Komaromi, I.; Martin, R. L.; Fox, D. J.; Keith, T.; Al-Laham, M. A.; Peng, C. Y.; Nanayakkara, A.; Challacombe, M.; Gill, P. M. W.; Johnson, B.; Chen, W.; Wong, M. W.; Gonzalez, C.; Pople, J. A. *Gaussian03*; Gaussian Inc.: Wellington, CT, 2004.
(48) Werner, H.-J.; Knowles, P. J.; Amös, R. D.; Bernhardsson, A.; Berning, A.; Celani, P.; Cooper, D. L.; Deegan, M. J. O.; Doobbyn, A. J.; Eckert, F.; Hampel, C.; Hetzer, G.; Korona, T.; Lindh, R.; Lloyd, A. W.; McNicholas, S. J.; Manby, F. R.; Meyer, W.; Mura, M. E.; Nicklass, A.; Palmieri, P.; Pitzer, R.; Rauhut, G.; Schütz, M.; Schumann, U.; Stroll, H.; Stone, A. J.; Tarroni, R.; Thorsteinsson, T. MOLPRO is a package of ab initio programs ver. version 2002.1, 1998.
(49) Klippenstein, S. J.; Wagner, A. F.; Dunbar, R. C.; Wardlaw, D. M.; Robertson, S. H.; Miller, J. A. VARIFLEX ver. 1.14m, 2005.
(50) Miller, J. A.; Klippenstein, S. J. *J. Phys. Chem. A* **2000**, *104*, 2061–2069.
(51) Senosiain, J. P.; Klippenstein, S. J.; Miller, J. A. 2008, unpublished results.
(52) Harding, L. B.; Klippenstein, S. J.; Jasper, A. W. *Phys. Chem. Chem. Phys.* **2007**, *9*, 4055–4070.
(53) Walsh, R. *Int. J. Chem. Kinet.* **1970**, *2*, 71–74.
(54) Robertson, S. H.; Pilling, M. J.; Jitariu, L. C.; Hillier, I. H. *Phys. Chem. Chem. Phys.* **2007**, *9*, 4085–4097.
(55) Senosiain, J. P.; Klippenstein, S. J.; Miller, J. A. *J. Phys. Chem. A* **2006**, *110*, 5772–5781.
(56) Kee, R. J.; Rupley, R. M.; Miller, J. A.; Coltrin, M. E.; Grcar, J. F.; Meeks, E.; Moffat, H. K.; Lutz, A. E.; Dixon-Lewis, G.; Smooke, M. D.; Warnatz, J.; Evans, G. H.; Larson, R. S.; Mitchell, R. E.; Petzold, L. R.; Reynolds, W. C.; Caracotsios, M.; Stewart, W. E.; Glarborg, P.; Wang, C.; Adigun, O.; Houf, W. G.; Chou, C. P.; Miller, S. F.; Ho, P.; Young, D. J. *Chemkin Release 4.1*; Reaction Design, Inc.: San Diego, CA, 2006.

JP804510K